Journal of Materials Chemistry A

Accepted Manuscript

ROYAL SOCIETY OF CHEMISTRY

www.rsc.org/materialsA

Journal of Materials Chemistry A

ARTICLE

An Aqueous, Organic Dye Derivatized SnO_2/TiO_2 Core/Shell Photoanode

Received 00th January 20xx,
Accepted 00th January 20xx

DOI: 10.1039/x0xx00000x

www.rsc.org/

Kyung-Ryang Wee,[a] Benjamin D. Sherman,[a] M. Kyle Brennaman,[a] Matthew V. Sheridan,[a] Animesh Nayak,[a] Leila Alibabaei,[a] and Thomas J. Meyer*[,a]

Visible light driven water splitting in a dye-sensitized photoelectrochemical cell (DSPEC) based on a phosphonic acid-derivatized donor-π-acceptor (D-π-A) organic dye (**P-A-π-D**) is described with the dye anchored to an FTO|SnO_2/TiO_2 core/shell photoanode in a pH 7 phosphate buffer solution. Transient absorption measurements on FTO|TiO_2|-[**P-A-π-D**] compared to core/shell, FTO|SnO_2/TiO_2(3nm)|-[**P-A-π-D**], reveal that excitation of the dye is rapid and efficient with a decrease in back electron rate by a factor of ~10 on the core/shell. Upon visible, 1 sun excitation (100 $mWcm^{-2}$) of FTO|SnO_2/TiO_2(3nm)|-[**P-A-π-D**] in a phosphate buffer at pH 7 with 20 mM added hydroquinone (H_2Q), photocurrents of ~2.5 mA/cm^2 are observed which are sustained over >15 min photolysis periods with a current enhancement of ~30-fold compared to FTO|TiO_2|-[**P-A-π-D**] due to the core/shell effect. On surfaces co-loaded with both -[**P-A-π-D**] and the known water oxidation catalyst, $Ru(bda)(pyP)_2$ (pyP = pyridin-4-methyl phosphonic acid), maximum photocurrent levels of 1.4 mA/cm^2 were observed which decreased over an 10 min interval to 0.1 mA/cm^2. O_2 was measured by use of a two-electrode, collector-generator sandwich cell and was produced in low Faradaic efficiencies with the majority of the oxidative photocurrent due to oxidative decomposition of the dye.

Introduction

The goal of artificial photosynthesis is to make high energy chemical fuels from solar energy. A promising, but still evolving, approach is the dye-sensitized photoelectrosynthesis cell (DSPEC). It integrates molecular light absorption and catalysis with high band gap metal oxide semiconductors.[1-6] A number of reports have appeared recently on DSPEC water splitting.[7-9] In these applications, Ru(II) polypyridyl complex derivatives of $Ru^{II}(bpy)_3^{2+}$ (bpy is 2,2`-bipyridine) have provided an ubiquitous class of photosensitizers for photoanode applications and water oxidation due to their favorable properties including stability in water and tunable light absorption and redox potentials.[10,11]

Examples of organic chromophores capable of driving water oxidation at DSPEC photoanodes are limited[12-16] even given the large portfolio of organic dyes developed for dye-sensitized solar cells (DSSCs).[16] In using these dyes, significant challenges arise from combining broad light absorption, efficient excited state injection, catalyst oxidation, and aqueous solution stability.[9,10, 17,18]

Here we describe the use of a common DSSC, donor-π-bridge-acceptor (D-π-A) dye in a DSPEC water splitting application. It consists of a triphenylamine electron donor, π-conjugated bridge, and electron acceptor derivatized with a phosphonate anchoring group, D-π-A-PO_3H_2 (**P-A-π-D**, Fig. 1b inset). It is one of a class of dyes that have been successfully used in DSSCs with efficiencies of >10% reported.[19-21] The electronic properties, stabilities, and photo-induced electron transfer properties of these dyes on TiO_2 are well known in organic solvents but only limited information is available in aqueous solutions.[22,23]

We report here, that when surface-bound on SnO_2/TiO_2 core-shell electrodes, with added hydroquinone (H_2Q) as a reductive electron transfer scavenger, the surface-bound dye gives rise to impressively high, sustained photocurrents. When co-loaded with a phosphonic acid-derivatized water oxidation catalyst, the dye has also been utilized in a DSPEC for visible light driven water splitting.

Results and discussion

In cyclic voltammograms (CV) of FTO|TiO_2|-[**P-A-π-D**] (~20 nm particle diameter, ~ 4 μm thick) in acetonitrile 0.1 M in TBAP as a function of scan rate, Fig. 1a, reversible, kinetically distorted waves appear at $E_{1/2}$ = 0.9 V and 1.4 V vs Ag/AgCl (Ag/AgCl, 3M KCl, 0.199 V vs. NHE). The scan rate dependences for both couples are consistent with kinetically inhibited, but relatively rapid cross-surface electron transfer across the semiconductor oxide electrode surface compared to Ru(II) polypyridyl complexes.[11] Complete oxidation to the dication, -[**P-A-π-D**] $\xrightarrow{-2e^-}$ -[**P-A-π-D**]$^{2+}$, during the CV scans was easily discerned by a reversible color change from the orange color of -[**P-A-π-D**] to the dark blue of -[**P-A-π-D**]$^+$ or -[**P-A-π-D**]$^{2+}$, inset, Fig. 1a. In acetonitrile, no significant reduction in current was observed even after 50 CV scan cycles at 20 mV/s, Fig. S1, highlighting the relative stability of the mono- and dicationic forms of the dye in acetonitrile with 0.1 M tetrabutylammonium hexafluorophosphate (TBAP) as the electrolyte.

[a] Department of Chemistry, University of North Carolina at Chapel Hill, Chapel Hill, North Carolina 27599, United States, E-mail: tjmeyer@unc.edu

Electronic Supplementary Information (ESI) available: [Experimental details of **P-A-π-D** based photoanode in pH 7 phosphate buffer are provided]. See DOI: 10.1039/x0xx00000x

UV-visible absorption spectra of the oxidized dye on TiO_2 in acetonitrile were obtained by spectroelectrochemical measurements obtained by using 30 mV-30 s potential step and hold increments from 0.4 to 2.0 V. The results are shown as difference spectra between final and initial spectra in Fig. 1b. They show that oxidation is accompanied by loss of the neutral dye absorption at ~450 nm and the appearance of new absorption features at 610 nm and 720 nm for both cations but with different molar absorptivities.[23]

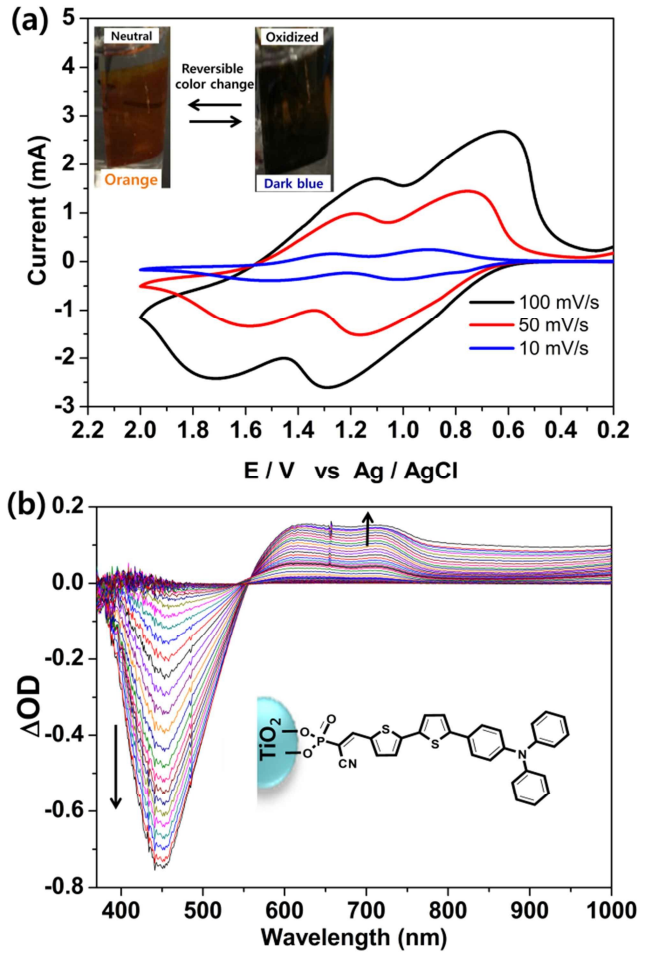

Figure 1. (a) Scan rate dependent CV traces for a FTO|TiO_2|-[**P-A-π-D**] film (~20 nm particle diameter, ~ 4 μm thick) as a function of scan rate with visual snapshots of the film illustrating the color change upon oxidation in acetonitrile 0.1 M in TBAP. (b) UV-visible difference spectra from spectroelectrochemical measurements at 30 mV increments from 0.4 V to 2.0 V.

The stability of electrochemically generated FTO|TiO_2|-[**P-A-π-D**]$^+$, at pH 7 in a 0.1 M $H_2PO_4^-/HPO_4^{2-}$ buffer solution in 0.5 M KNO_3, was monitored by repetitive CV scans. As shown in Fig. S2, at a scan rate of 20 mV/s, the -[**P-A-π-D**]$^{+/0}$ couple is chemically reversible but the -[**P-A-π-D**]$^{2+/+}$ couple is irreversible. The long-term stability of FTO|TiO_2|-[**P-A-π-D**]$^+$ at pH 7 in the phosphate buffer was further investigated by carrying out a sequence of successive CV scans at 50 mV/s with the degree of electron transfer reversibility for the -[**P-A-π-D**]$^{+/0}$ couple monitored by cathodic peak current measurements following oxidative scans through the -[**P-A-π-D**]$^{+/0}$ wave, Fig. S3. In contrast to acetonitrile, oxidation to the mono-cation results in slow decomposition under these conditions, Fig. S3.

$$\text{FTO}|\text{SnO}_2/\text{TiO}_2(3\text{nm})|\text{-[P-A-}\pi\text{-D]} \xrightarrow{h\nu} \text{FTO}|\text{SnO}_2/\text{TiO}_2(3\text{nm})|\text{-[P-A-}\pi\text{-D]}^* \quad (1)$$

$$\text{FTO}|\text{SnO}_2/\text{TiO}_2(3\text{nm})|\text{-[P-A-}\pi\text{-D]}^* \xrightarrow{injection} \text{FTO}|\text{SnO}_2/\text{TiO}_2(3\text{nm})(e^-)|\text{-[P-A-}\pi\text{-D]}^+ \quad (2)$$

$$\text{FTO}|\text{SnO}_2(e^-)/\text{TiO}_2(3\text{nm})|\text{-[P-A-}\pi\text{-D]}^+ \xrightarrow{k_{bet}} \text{FTO}|\text{SnO}_2/\text{TiO}_2(3\text{nm})|\text{-[P-A-}\pi\text{-D]} \quad (3)$$

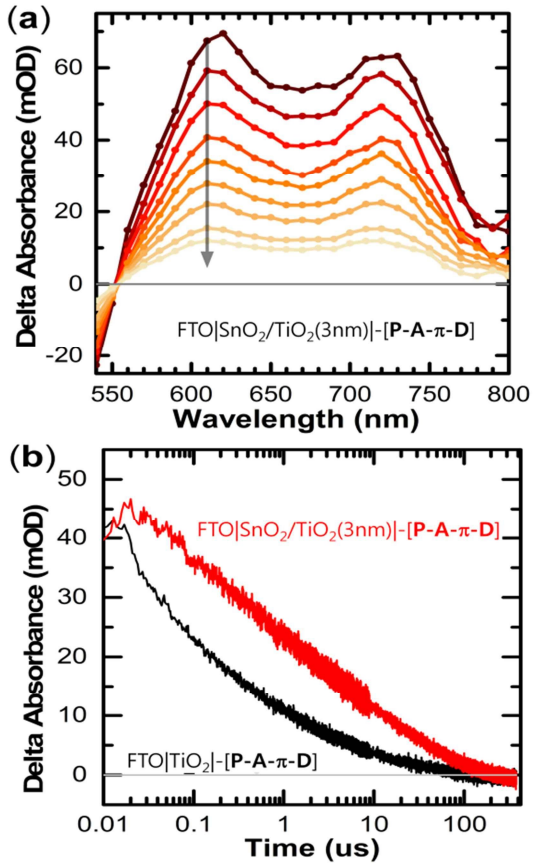

Figure 2. (a) Transient absorption difference spectra for FTO|SnO_2/TiO_2(3nm)|-[**P-A-π-D**] in pH 7 phosphate buffer in 0.5 M KNO_3 following 5 ns, 3.1 mJ, 425 nm laser excitation. Spectral changes are indicated by the gray arrow and are shown from 20 ns after the laser pulse (darkest red) to 8.6 μs (lightest orange) with intermediate spectra at 50 ns, 100 ns, 250 ns, 1 μs, 2 μs, and 5 μs. (b) Transient absorption-time traces at 610 nm comparing on FTO|SnO_2/TiO_2(3nm) (red) and on FTO|TiO_2 (black) with the laser pulse excitation energy adjusted to generate the same amplitude change for both samples at the earliest observation time of 10 ns.

Injection and back electron transfer were investigated for the dye fully-loaded on nanoparticle TiO_2, FTO|TiO_2|-[**P-A-π-D**], and core/shell SnO_2/TiO_2(3nm), FTO|SnO_2/TiO_2(3nm)|-[**P-A-π-D**] by nanosecond transient absorption (TA) measurements. As described previously,[24] the core/shell consisted of an inner core of ~20 nm particle diameter, ~ 4 μm thick SnO_2 with 3 nm outer shells of TiO_2 deposited by atomic layer deposition (ALD). The transient

absorption (TA) measurements were carried out in a pH 7 phosphate buffer in 0.5 M KNO_3. From the absence of measurable emission, electron injection by the dye is efficient on both oxides. In these experiments, transient absorption difference spectra were acquired following 425 nm excitation. Difference spectra from 550 to 800 nm at various time intervals from 20 ns to 8.6 μs after the laser pulse are shown in Fig. 2.

Injection on both oxides was complete on the ~20 nsec timescale of the TA measurements. There was clear evidence in the transient spectra for -[**P-A-π-D**]$^+$ by the appearance of its characteristic absorption features at 610 and 720 nm and, in the time evolution of the difference spectra, for the excitation/injection/back electron transfer sequence in eqs 1-3. As shown by analysis of transient absorption-time traces at 610 or 720 nm, the kinetics of back electron transfer, eq 3, were highly non-exponential. The time for half the total absorbance change to occur at either monitoring wavelength was $t_{1/2}$ = 1.02 μs on the core/shell oxide and $t_{1/2}$ = 170 ns on TiO_2. The significant decrease in $t_{1/2}$ for back electron transfer on the core/shell electrode is notable and consistent with earlier observations.[24] Back electron transfer to the assembly through the SnO_2/TiO_2 core/shell, eq 3, is inhibited by the ~0.4 V offset in band gap potentials between the oxides.

Photocurrent-time measurements for FTO|TiO_2|-[**P-A-π-D**] and FTO|SnO_2/TiO_2(3nm)|-[**P-A-π-D**] (~20 nm particle diameter, ~ 8 μm thick) in the pH 7 phosphate buffer were measured with an external bias of 0.2 V vs SCE and an external Pt cathode. The linear scan voltammetric (LSV) traces for FTO|TiO_2|-[**P-A-π-D**] and FTO|SnO_2/TiO_2(3nm)|-[**P-A-π-D**] under dark and light conditions are shown in Fig. 3b inset and Fig. S4-S5. The preparation, characterization and use of the SnO_2/TiO_2 electrode in DSPEC water splitting applications was described in a previous publication.[24] Photolysis of the derivatized core/shell electrode at the photolysis steady state resulted in a noticeable color change, consistent with the appearance of -[**P-A-π-D**]$^+$ on the surface (Fig. S6). In the photoelectrochemical experiments, H_2Q, was added as an irreversible electron transfer scavenger for the monocation as it forms with the effect maximized by 20 mM added H_2Q. As shown in eq 4, H_2Q is oxidized by -[**P-A-π-D**]$^+$ to give the semiquinone, $HQ^{\cdot}$, followed by its rapid disproportionation to Q + H_2Q.[25]

Fig. 3a illustrates photocurrent-time traces with and without added H_2Q for both derivatized electrodes with 100 mWcm^{-2} white light (~1 sun) irradiation and a 400 nm cut-off filter as described previously.[18] An initial photocurrent density of ~0.5 mA/cm^2 was observed for FTO|SnO_2/TiO_2(3nm)|-[**P-A-π-D**] and only a few μA/cm^2 for FTO|TiO_2|-[**P-A-π-D**]. The large initial photocurrent spikes, which occur on the seconds timescale, have been attributed to oxidation of the surface-bound assemblies and equilibration of the local /double layer.[26] At the end of the photolysis periods negative photocurrent spikes appeared on the same seconds timescale consistent with back electron transfer to the film and re-equilibration of the double layer.

As shown by the data in Fig 3a, greatly enhanced photocurrents are observed for FTO|SnO_2/TiO_2(3nm)|-[**P-A-π-D**] with added H_2Q. Photocurrent levels reach ~2.5 mA/cm^2 with no initial current spike, consistent with rapid reduction of -[**P-A-π-D**]$^+$ by H_2Q, eq 4, before double layer equilibration can occur, Fig. 3a. During 30 s illumination periods, the photocurrent increased slightly with reproducible current-time traces obtained for multiple (30 s light on/off) cycles.

The results of incident photon to current efficiency (IPCE) measurements on FTO|SnO_2/TiO_2(3nm)|-[**P-A-π-D**] with added H_2Q are shown in Fig. S7. The match with the absorption spectrum of **P-A-π-D** shows that chromophore excitation and injection are the origin of the observed photocurrents. Given the 8 μm film thickness, with nearly complete light absorption by the dye at λ_{max} ~ 450 nm, the absorbed photon to current efficiency (APCE) at this wavelength is ~17%. Under these conditions the FTO|SnO_2/TiO_2(3nm)|-[**P-A-π-D**] electrode acts as a DSPEC photoanode for the net dehydrogenation of hydroquinone, H_2Q + 2 *hν* → Q + H_2, with H_2 produced at the cathode by H_2O reduction, eq 4.

Photoanode:

FTO|$SnO_2(e^-)/TiO_2$(3nm)|-[**P-A-π-D**]$^+$ + ½H_2Q $\xrightarrow{h\nu}$ FTO|$SnO_2(e^-)/TiO_2$(3nm)|-[**P-A-π-D**] + ½Q +H^+

Cathode: 2 $H_2PO_4^-$ + 2e^- → H_2 + 2HPO_4^{2-} (4)

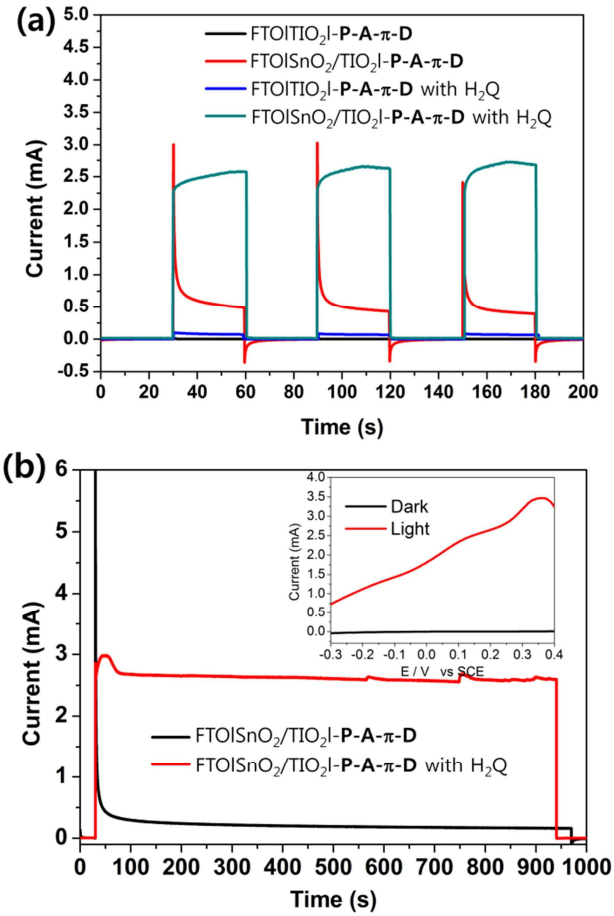

Figure 3. (**a**) Photocurrent-time traces with 30 second light off/on cycles for FTO|TiO_2|-**P-A-π-D** (black), FTO|SnO_2/TiO_2(3nm)|-**P-A-π-D** (red), and for FTO|TiO_2|-**P-A-π-D** with 20 mM added H_2Q (blue); and for FTO|SnO_2/TiO_2(3nm)|-**P-A-π-D** with added H_2Q (cyan): 0.2 V bias vs. SCE in 0.1 M pH 7 phosphate buffer in 0.5 M KNO_3 with 100 mW cm^{-2} light illumination and a 400 nm long-pass filter. (**b**) Photocurrent traces for FTO|SnO_2/TiO_2(3nm)|-[**P-A-π-D**] with (red) and without (black) added H_2Q over 15 min photolysis periods. (Inset: LSV traces for FTO|SnO_2/TiO_2(3nm)|-[**P-A-π-D**] with 20 mM added H_2Q under dark and light conditions; scan rate = 20 mV/s.)

Based on the 100 mW/cm^2 white light (~1 sun) excitation source and sustained photocurrents of ~2.5 mA/cm^2, the solar

photocurrent efficiency with added H_2Q is ~6%. The impact of the core/shell structure is profound as seen in the photocurrent comparison with FTO|TiO_2|-[**P-A-π-D**] in Fig. 3a with a decrease in photocurrent to ~5 μA/cm^2 for the assembly on TiO_2.[24]

During a 30 s illumination period, the photocurrent with added H_2Q increased slightly with reproducible current-time traces obtained during multiple (30 s light on/off) cycles. Over a 15 min photolysis period (Fig. 3b), ~98 % of the initial photocurrent was maintained at the end of the photolysis period.

The four electron/four proton dehydrogenation of water to O_2 (water splitting, eq. 5) is more challenging than dehydrogenation of hydroquinone, requiring four excitation/injection cycles. In order to explore possible light-driven water oxidation by the organic dye, a chromophore-catalyst assembly was prepared by co-loading the dye with the water oxidation catalyst Ru(bda)(pyP)$_2$ (bda = 2,2'-bipyridine-6,6'-dicarboxylate, pyP = pyridin-4-methyl phosphonic acid) at a 5:1 ratio on the ~8 μm SnO_2/TiO_2(3nm) core/shell electrodes.[27] The catalyst is a member of a class of water oxidation catalysts described by Sun and co-workers.[28,29] (Fig. 4 inset) As shown in Fig. S8, CV data on FTO electrodes co-loaded with -**P-A-π-D** and -Ru(bda)(pyP)$_2$ at a 5:1 ratio provides direct evidence for mediated electron transfer activation of the catalyst by the oxidized dye on the oxide surface with an onset potential of ~0.65 V vs. AgCl/Ag.[31]

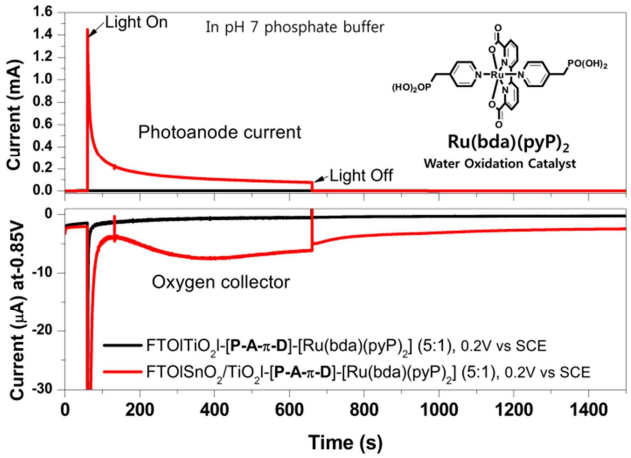

Figure 4. Upper: current–time trace (60–600 s) at illuminated (1 sun, 100 mWcm^{-2}; 400 nm cut-off filter) [**P-A-π-D**]-[Ru(bda)(pyP)$_2$] (5:1 ratio) on FTO|TiO_2 (black line) and on FTO|SnO_2/TiO_2(3nm) (red line) in 0.1 M phosphate buffer at pH 7 with an applied bias of 0.2 V versus SCE. Lower: current-time traces at an FTO collector electrode, ~1 mm from the photoanode at an applied bias of -0.85 V versus SCE measured concurrently with the photoelectrochemical-time trace. See SI for details.

As shown in Fig. 4, co-loading of **P-A-π-D** and Ru(bda)(pyP)$_2$ on a ~8 μm SnO_2/TiO_2(3nm) core/shell electrode at a 5:1 ratio gives sustained photocurrents under white light illumination (1 sun, 100 mW cm^{-2}). Following the initial photocurrent spike with ~1.4 mA, the photocurrent gradually decreased to 0.1 mA/cm^2 after 60 s far less than the ~2.5 mA/cm^2 observed with added H_2Q. The same surface assembly on TiO_2 gave a negligible photoresponse. Oxygen produced during the photolysis period was measured directly by using a collector-generator technique in which a second, FTO working electrode was positioned 1 mm from the photoanode to monitor O_2 as it was produced. The collector-generator technique was described previously.[30,31] The **P-A-π-D** dye only on a SnO_2/TiO_2(3nm) core/shell (Fig. S9) gave a negligible O_2 current.

Based on the collector-generator current results in Fig. 4, O_2 is not produced at FTO|TiO_2|-[**P-A-π-D**]-[Ru(bda)(pyP)$_2$] (5:1 ratio) in measurable quantities, in part, due to the low photocurrents and competitive back electron transfer with TiO_2 as the oxide. O_2 is produced at the core/shell electrode with considerably enhanced photocurrents. However, from the total charge passed during the illumination period, the faradaic efficiency for O_2 production was only 8.2%. Similar observations have been made for Ru(II) polypyridyl-based chromophores and attributed to oxidative decomposition of the chromophore.[30] Photochemical decomposition of the dye is also apparent in the low but sustained photocurrents observed for FTO|SnO_2/TiO_2(3nm)|-[**P-A-π-D**] with no added water oxidation catalyst in Fig. 3a. Oxidatively-induced decomposition of the organic dye in the FTO|SnO_2/TiO_2(3nm)|-[**P-A-π-D**] film at the dithiophene unit is the origin of the sustained photocurrents with no O_2 production and is currently under investigation.

Limited O_2 production and low photocurrents for the assembly electrode, FTO|SnO_2/TiO_2(3nm)|-[**P-A-π-D**]-[Ru(bda)(pyP)$_2$], is in marked contrast to the relatively high efficiency for H_2Q oxidation at FTO|SnO_2/TiO_2(3nm)|-[**P-A-π-D**] highlighting the challenges arising in DSPEC water splitting from the requirements for multiple excitation/activation cycles. Although the core/shell structure provides an efficient basis for single photon/single electron activation of the catalyst through the known activation sequence, Ru(II) $\xrightarrow{h\nu,-e^-}$ Ru(III) $\xrightarrow{h\nu,-e^-}$ Ru(IV) $\xrightarrow{h\nu,-e^-}$ Ru(V),[32,33] subsequent water oxidation by Ru(V), is relatively slow. With this interpretation, the origin of the low Faradaic yield for O_2 evolution is slow water oxidation by the catalyst which is in competition with -[**P-A-π-D**]$^+$ decomposition.

Conclusions

Our results are encouraging in demonstrating the use of a D-π-A organic dye as a photosensitizer in a DSPEC photoanode with a high and sustained photocurrent density in an aqueous solution. Photoelectrochemical water oxidation for the co-loaded core/shell assembly, FTO|SnO_2/TiO_2(3nm)|-[**P-A-π-D**]-[Ru(bda)(pyP)$_2$], does occur but, due to slow water oxidation, with a low Faradaic efficiency for O_2 production. The stability and interfacial photodynamics of **P-A-π-D** dyes on metal oxide surfaces under a variety of conditions are currently under investigation, as is optimization of the D-π-A molecular structure to achieve efficient, stable DSPEC water splitting.

Experimental

General. Diethyl cyanomethylphosphonate (98%), trimethylsilyl iodide (97%), trimethylsilyl bromide (97%), piperidine (99%), and all reagents or solvents were obtained from either Sigma-Aldrich or Fisher Scientific and used without any purification. Aqueous solutions were prepared from water purified by a Millipore Milli-Q Synthesis A10 purification system. Deuterated solvent $CDCl_3$, CD_3OD, and DMSO for NMR were obtained from Cambridge Isotope Laboratories Inc. The ^{1}H, ^{13}C, and ^{31}P spectra were recorded on a Bruker 400 spectrometer and all proton and carbon chemical shifts

were measured relative to internal residual chloroform (99.5% $CDCl_3$) or CD_3OD or DMSO from the lock solvent. The acid protons for **P-A-π-D** and Ru(bda)$(pyP)_2$ are not detected by ^{1}H-NMR.

5′-(4-(Diphenylamino)phenyl)-2,2′-bithiophene-5-carbaldehyde. The aldehyde precorsor was synthesized using a previous published method.[34]

(E)-diethyl 1-cyano-2-(5'-(4-(diphenylamino)phenyl)-2,2'-bithiophen-5-yl)vinylphosphonate (OrgD-POEt). A solution of aldehyde precorsor (1.00 g, 2.28 mmol), diethyl cyanomethylphosphonate (0.45 g, 2.51 mmol), and piperidine (0.25 mL, 2.51 mmol) in MeCN (70 ml) was heated to reflux for overnight and cooled to room temperature. The residue was diluted with water and extracted with CH_2Cl_2. The combined organic layer was dried over anhydrous $MgSO_4$ and filtered off. After removal of the solvent under reduced pressure, silica-gel column chromatography of the residue with CH_2Cl_2 as eluent gave the product OrgD-POEt as a red powder. Yield: 1.01 g (74%). ^{1}H NMR ($CDCl_3$): δ 8.05 (d, 1 H), 7.60 (d, 1 H), 7.48 (d, 2 H), 7.36 (d, 1 H), 7.31, (t, 4 H), 7.24 (d, 1 H), 7.20 (d, 1 H), 7.15 (d, 4 H), 7.08 (m, 4 H), 4.24 (m, 4 H), 1.43 (t, 6 H). ^{13}C NMR ($CDCl_3$): δ 150.2, 148.1, 147.2, 146.9, 146.5, 138.3, 135.0, 134.8, 133.8, 129.4, 127.5, 127.0, 126.6, 124.8, 123.7, 123.5, 123.3, 123.1, 116.1. 63.5, 16.3. ^{31}P NMR ($CDCl_3$): δ 12.22. Anal. Found (Calc) for $C_{33}H_{29}N_2O_3PS_2$: C, 66.52 (66.42); H, 4.95 (4.90); N, 4.73 (4.69).

(E)-1-cyano-2-(5'-(4-(diphenylamino)phenyl)-2,2'-bithiophen-5-yl)vinylphosphonic acid (P-A-π-D). OrgD-POEt (0.6 g, 1.00 mmol) was dissolved in anhydrous CH_2Cl_2 (70 mL) under an atmosphere of argon. To the solution was added trimethylsilyl bromide (0.30 mL, 2.20 mmol), and the reaction was stirred at room temperature under an atmosphere of argon for overnight. The solvent was removed under vacuum, and anhydrous methanol (10 mL) was added. The methanol was removed under vacuum after stirred for 30 min at room temperature. **P-A-π-D** was purified by silica gel column chromatography using CH_2Cl_2/MeOH (2:1) as the eluent and deep red powder was obtained. Yield: 0.36 g (67%). ^{1}H NMR (DMSO): δ 7.95 (d, 1 H), 7.77 (d, 1 H), 7.58 (d, 2 H), 7.49-7.25 (m, 7 H), 7.11-6.81 (m, 8 H). ^{13}C NMR (DMSO): δ 147.8, 147.1, 146.5, 146.4, 145.1, 135.7, 130.1, 129.1, 128.1, 127.0, 125.9, 125.0, 124.7, 124.6, 124.1, 124.0 122.9, 122.6, 100.0. ^{31}P NMR (DMSO): δ 5.17. Anal. Found (Calc) for $C_{29}H_{21}N_2O_3PS_2$: C, 64.31 (64.43); H, 3.89 (3.92); N, 5.23 (5.18).

Oxidation catalyst of Ru(bda)$(pyPO_3Et_2)_2$. The water oxidation catalyst of Ru(bda)$(pyP)_2$ (bda = 2,2'-bipyridine-6,6'-dicarboxylate, pyP = pyridin-4-ylmethylphosphonic acid) was prepared according to previously published procedures.[27] A solution of [Ru(η^6-benzene)$(Cl)_2]_2$ (100 mg, 0.19 mmol) and 2,2'-bipyridine-6,6'-dicarboxylate (bda, 95 mg, 0.39 mmol) in distilled MeOH (30 ml) was heated to reflux for 2 h. After cool down to room temperature, diethyl pyridin-4-ylmethylphosphonate (230 mg, 1.00 mmol) and NEt_3 (0.4 ml) was added and then refluxed for overnight. After removal of the solvent under reduced pressure, the residue was diluted with CH_2Cl_2 and then excess hexane was poured to form a precipitate. The precipitate was filtered off and dried under reduced pressure to give a dark black powder. Yield: 120 mg (39%). ^{1}H NMR (MeOD): δ 8.60 (d, 2 H), 8.04 (d, 2 H), 7.89 (t, 2 H), 7.66 (d, 4 H), 7.05 (d, 4 H), 4.13 (m, 8 H), 3.42 (s, 4 H). 1.35 (t, 12 H). ^{31}P NMR (MeOD): δ 22.22. Anal. Found (Calc) for $C_{32}H_{38}N_4O_{10}P_2Ru$: C, 47.79 (47.94); H, 4.81 (4.78); N, 6.87 (6.99).

Oxidation catalyst of Ru(bda)$(pyP)_2$. The Ru(bda)$(pyPO_3Et_2)_2$ (100 mg, 0.12) was dissolved in CH_2Cl_2 and trimethylsilyl iodide (TMSI, 0.14 ml, 1.00 mmol) was slowly added at room temperature. After overnight, an excess MeOH was added to the mixture and dried under vaccum. The result powder was washed with CH_2Cl_2/hexane (2:1) mixture solvent and dark black powder was obtained. Yield: 43 mg (51%). ^{1}H NMR (DMSO): δ 9.16 (d, 2 H), 8.17 (d, 2 H), 8.03 (t, 2 H), 7.55 (d, 4 H), 7.15 (d, 4 H), 3.11 (s, 4 H). ^{31}P NMR (DMSO): δ 18.17. Anal. Found (Calc) for $C_{24}H_{22}N_4O_{10}P_2Ru$: C, 41.64 (41.81); H, 3.25 (3.22); N, 8.15 (8.13).

Metal-Oxide Film Preparation. Mesoporous titanium dioxide nanoparticle films (TiO_2, ~20 nm particle diameter, ~ 8 μm thickness for photocurrent experiment or ~4 μm thickness for CV and TA experiment, 1×1 cm^2) and SnO_2,/(3nm)TiO_2 core-shell nanoparticle films (SnO_2 core, ~20 nm particle diameter, ~ 8 μm thickness for photocurrent experiment or ~4 μm thickness for TA experiment, 1×1 cm^2) were prepared, according a literature procedure,[24,31,35,36] onto an area of 10 mm × 25 mm on top of fluoride-doped tin oxide (FTO)-coated glass electrode (Hartford Glass; sheet resistance 15 Ω cm^{-2}). ALD was performed using a Cambridge NanoTech Savannah S200 instrument with TDMAT (tetrakis(dimethylamino)titanium) as Ti precursor for the SnO_2/TiO_2 core-shell electrode. **P-A-π-D** dye molecule absorption and CV data in CH_2Cl_2 solutions are shown in Fig. S14. Metal oxide-coated electrodes were derivatized by soaking in 2.0 mM **P-A-π-D** CH_2Cl_2 solutions overnight followed by neat CH_2Cl_2 soaking for an additional 12 h to remove any loosely bound **P-A-π-D**. The **P-A-π-D** undergoes stable surface binding to nanocrystalline, nanoparticle TiO_2 films and other oxides with a maximum surface coverage in a TiO_2 film of Γ_{max} = 2.4 × 10^{-7} mol cm^{-2}. (Fig. S15) Relative surface coverage of **P-A-π-D** and Ru(bda)$(pyP)_2$ was controlled by loading times in the two solutions. Surface coverages of each molecule (Γ in mol cm^{-2}) were determined from Beer's Law with absorbance measurements at two different wavelengths using the molar absorptivities.

Photophysical and Electrochemical Measurements. Absorption spectra were obtained by placing the dry, derivatized films perpendicular to the detection beam path of the spectrophotometer using an Agilent Cary 60 UV–vis spectrophotometer. The expression, $\Gamma = A(\lambda)/\varepsilon(\lambda_{480nm})/1000$, was used to calculate surface coverage. Electrochemical measurements (Cyclic Voltammetry, CV) were conducted by using a CH Instruments 660D potentiostat with a Pt-mesh or Pt-wire counter electrode, and an Ag/AgCl (3M KCl, 0.199 V vs. NHE) reference electrode. CV was performed for acetonitrile (ACN) solutions containing 0.1 M TBAP or pH 7 phosphate buffer aqueous solution containing 0.1 M $H_2PO_4^-$ /HPO_4^{2-}, 0.5 M KNO_3 at room temperature under argon.

Nanosecond Transient Absorption Spectroscopy. These measurements were conducted by using an experimental apparatus previously described.[37] Transient absorption measurements used a commercially available laser flash photolysis apparatus (Edinburgh Instruments, Inc., model LP920) with laser excitation (425 nm, 3.2 mJ, 8-mm diameter, 5–7-ns FWHM) provided by a pulsed neodymiumdoped yttrium aluminum garnet (Spectra-Physics, Inc., model Quanta-Ray LAB-170-10)/optical parametric oscillator (VersaScan-MB) laser combination. The repetition rate of the laser was matched to the rate at which the probe source was pulsed (i.e., intensified 50-fold compared with nonpulsed output), typically 1 Hz, although the laser flashlamps were fired at 10 Hz. Timing of the experiment was PC controlled via Edinburgh software (L900). The white light output of the LP920 probe source, a 450-W Xe lamp, was passed through a 40-nm long-pass color filter before passing through the sample. The LP920 was equipped with a multigrating detection monochromator outfitted with a Hamamatsu R928 photomultiplier tube (PMT) in a noncooled housing and a gated CCD (Princeton Instruments, PI-MAX3). The detector was software

selectable with the PMT for monitoring transient absorption kinetics at a single wavelength (10-ns FWHM instrument response function, reliable data out to 400 μs, 300–900 nm) and the gated CCD for transient spectra covering the entire visible region (400–850 nm) at a given time after excitation with a typical gatewidth of 10 ns. For PMT measurements, spectral bandwidth was typically <5 nm with color filters placed after the sample but before the detection monochromator to eliminate laser scatter. Single wavelength kinetic data were collected by averaging 10–100 sequences where one sequence refers to collection of laser-only data followed by pump–probe data. For timescales >10 μs, the probe-only data were also collected within the sequence because the strategy of using the linear portion before excitation to extrapolate the light intensity in the absence of the laser pulse was no longer valid due to a nonlinear temporal output of the pulsed probe source when viewed on longer timescales. Kinetic data were analyzed by using SigmaPlot (Systat, Inc.), Origin (OriginLab, Inc.), or L900 (Edinburgh, Inc.) software. Data were collected at room temperature (22 ± 1 °C).

Generator/collector O_2 detection. The generator/collector experiments for O_2 detection used a four electrode setup along with a bipotentiostat. Two FTO working electrodes in conjunction with a Pt counter and SCE reference electrode were used. One FTO (generator) electrode was prepared as described for the TiO_2 or SnO_2/(3nm)TiO_2 core/shell photoanodes used in this study; the other FTO (collector) electrode was unmodified. Assembly of the generator/collector setup involved placing the two FTO electrodes with the conductive sides facing with narrow 1 mm thick glass spacers between the lateral edges and sealing the sides with epoxy (Hysol). Prepared in this way, space between the two FTO electrodes will fill with electrolyte by capillary action when the cell is placed in solution. A Thor Labs HPLS 30-04 light source was used to provide white light illumination and a Lumencor Spectra Light Engine LED sources was used for 450 nm illumination. For all indicated experiments using 100 mW cm^{-2} white light illumination, the electrochemical cell was positioned an appropriate distance from the light source to receive the indicated light intensity as measured with a photodiode (Newport) and a 400 nm cutoff filter (Newport) was used to prevent direct bandgap excitation of the semiconductor layer. To measure the faradaic efficiency for O_2 production, the charge passed at the generator electrode during the illumination phase of the experiment was compared to the total charge passed at the collector electrode (poised at -0.85 V vs. SCE) during the entire experiment. The faradaic efficiency was corrected for the collection efficiency of the generator/collector setup (70%) that was determined experimentally.[30,31] The LSV traces of collector-generator electrodes for FTO|TiO_2|-[**P-A-π-D**]-[Ru(bda)(pyP)$_2$] (5:1 ratio) and FTO|SnO_2/TiO_2(3nm)|-[**P-A-π-D**]-[Ru(bda)(pyP)$_2$] (5:1 ratio) under dark and light conditions are shown in Fig. S16.

Acknowledgements

This material is based upon work solely supported as part of the UNC EFRC: Center for Solar Fuels, an Energy Frontier Research Center funded by the U.S. Department of Energy, Office of Science, Office of Basic Energy Sciences under Award Number DE-SC0001011.

Notes and references

1. M. G. Walter, E. L. Warren, J. R. McKone, S. W. Boettcher, Q. Mi, E. A. Santori, N. S. Lewis, *Chem. Rev.* **2010**, *110*, 6446.
2. J. J. Concepcion, R. L. House, J. M. Papanikolas, T. J. Meyer, *J. Proc. Natl. Acad. Sci.* **2012**, *109*, 15560.
3. J. R. Swierk, T. E. Mallouk, *Chem. Soc. Rev.* **2013**, *42*, 2357.
4. J. A. Treadway, J. A. Moss, T. J. Meyer, *Inorg. Chem.* **1999**, *38*, 4386.
5. J. H. Alstrum-Acevedo, M. K. Brennaman, T. J. Meyer, *Inorg. Chem.* **2005**, *44*, 6802.
6. W. J. Song, Z. F. Chen, M. K. Brennaman, J. J. Concepcion, A. O. T. Patrocinio, N. Y. M. Iha, T. J. Meyer, *Pure Appl. Chem.* **2011**, *83*, 749.
7. W. J. Youngblood, S.-H. A. Lee, Y. Kobayashi, E. A. Hernandez-Pagan, P. G. Hoertz, T. A. Moore, A. L. Moore, D. Gust, T. E. Mallouk, *J. Am. Chem. Soc.* **2009**, *131*, 926.
8. Y. Gao, X. Ding, J. Liu, L. Wang, Z. Lu, L. Li, L. Sun, *J. Am. Chem. Soc.* **2013**, *135*, 4219.
9. L. Alibabaei, M. K. Brennaman, M. R. Norris, B. Kalanyan, W. Song, M. D. Losego, J. J. Concepcion, R. A. Binstead, G. N. Parsons, T. J. Meyer, *Proc. Natl. Acad. Sci.* **2013**, *110*, 20008.
10. D. L. Ashford, M. K. Brennaman, R. J. Brown, S. Keinan, J. J. Concepcion, J. M. Papanikolas, J. L. Templeton, T. J. Meyer, *Inor. Chem.* **2015**, *54*, 460.
11. K. Hanson, M. K. Brennaman, A. Ito, H. Luo, W. Song, K. A. Parker, R. Ghosh, M. R. Norris, C. R. K. Glasson, J. J. Concepcion, R. Lopez, T. J. Meyer, *J. Phy. Chem. C* **2012**, *116*, 14837.
12. J. R. Swierk, D. D. Mendez-H., N. S. McCool, P. Liddell, Y. Terazono, I. Pahk, J. J. Tomlin, N. V. Oster, T. A. Moore, A. L. Moore, D. Gust, T. E. Mallouk, *Proc. Natl. Acad. Sci.* **2015**, *112*, 1681.
13. J. T. Kirner, J. J. Stracke, B. A. Gregg, R. G. Finke, *ACS Appl. Mater. Interfaces* **2014**, *6*, 13367.
14. F. Ronconi, Z. Syrgiannis, A. Bonasera, M. Prato, R. Argazzi, S. Caramori, V. Cristino, C. A. Bignozzi, *J. Am. Chem. Soc.* **2015**, *137*, 4630.
15. F. Li, K. Fan, B. Xu, E. Gabrielsson, Q. Daniel, L. Li, L. Sun, *J. Am. Chem. Soc.* **2015**, *137*, 9153.
16. A. Mishra, M. K. R. Fischer, P. Buerle, *Angew. Chem. Int. Ed.* **2009**, *48*, 2474.
17. K. Hanson, M. D. Losego, B. Kalanyan, G. N. Parsons, T. J. Meyer, *Nano Lett.* **2013**, *13*, 4802.
18. K.-R. Wee, M. K. Brennaman, L. Alibabaei, B. H. Farnum, B. Sherman, A. M. Lapides, T. J. Meyer, *J. Am. Chem. Soc.* **2014**, *136*, 13514.
19. Y. Wu, W.-H. Zhu, S. M. Zakeeruddin, M. Grätzel, *ACS Appl. Mater. Interfaces* **2015**, *7*, 9307.
20. J. Yang, P. Ganesan, J. Teuscher, T. Moehl, Y. J. Kim, C. Yi, P. Comte, K. Pei, T. W. Holcombe, M. K. Nazeeruddin, J. Hua, S. M. Zakeeruddin, H. Tian, M. Grätzel, *J. Am. Chem. Soc.* **2014**, *136*, 5722.
21. N. Zhou, K. Prabakaran, B. Lee, S. H. Chang, B. Harutyunyan, P. Guo, M. R. Butler, A. Timalsina, M. J. Bedzyk, M. A. Ratner, S. Vegiraju, S. Yau, C.-G. Wu, R. P. H. Chang, A. Facchetti, M.-C. Chen, T. J. Marks, *J. Am. Chem. Soc.* **2015**, *137*, 4414.
22. F. Bella, C. Gerbaldi, C. Barolob, M. Grätzel, *Chem. Soc. Rev.* **2015**, *44*, 3431.
23. W.-S. Han, K.-R. Wee, H.-Y. Kim, C. Pac, Y. Nabetani, D. Yamamoto, T. Shimada, H. Inoue, H. Choi, K. Cho, S. O. Kang, *Chem. Eur. J.* **2012**, *18*, 15368.
24. L. Alibabaei, B. D. Sherman, M. R. Norris, M. K. Brennaman, T. J. Meyer, *Proc. Natl. Acad. Sci.* **2015**, *112*, 5899.
25. H.-D. Becker, *J. Org. Chem.* **1967**, *32*, 2136.
26. J. R. Swierk, N. S. McCool, T. P. Saunders, G. D. Barber, T. E. Mallouk, *J. Am. Chem. Soc.* **2014**, *136*, 10974.

27. Y. Gao, L. Zhang, X. Dinga, L. Sun, *Phys. Chem. Chem. Phys.* **2014**, *16*, 12008.
28. L. Duan, F. Bozoglian, S. Mandal, B. Stewart, T. Privalov, A. Llobet, L. Sun, *Nat. Chem.* **2012**, *4*, 418.
29. Y. Gao, X. Ding, J. Liu, L. Wang, Z. Lu, L. Li, L. Sun, *J. Am. Chem. Soc.* **2013**, *135*, 4219.
30. D. L. Ashford, B. D. Sherman, R. A. Binstead, J. L. Templeton, T. J. Meyer, *Angew. Chem. Int. Ed.* **2015**, *54*, 4778.
31. B. D. Sherman, D. L. Ashford, A. M. Lapides, M. V. Sheridan, K.-R. Wee, T. J. Meyer, *J. Phys. Chem. Lett.* **2015**, *6*, 3213
32. N. Song, J. J. Concepcion, R. A. Binstead, J. A. Rudd, A. K. Vannucci, C. J. Dares, M. K. Coggins, T. J. Meyer, *Proc. Natl. Acad. Sci.* **2015**, *112*, 1681.
33. M. V. Sheridan, B. D. Sherman, Z. Fang, K.-R. Wee, M. K. Coggins, T. J. Meyer, *ACS Catal.* **2015**, *5*, 4404.
34. K. R. J. Thomas, Y.-C. Hsu, J. T. Lin, K.-M. Lee, K.- C. Ho, C.-H. Lai, Y.-M. Cheng, P.-T. Chou, *Chem. Mater.* **2008**, *20*, 1830.
35 S.-H. A. Lee, N. M. Abrams, P. G. Hoertz, G. D. Barber, L. I. Halaoui, T. E. Mallouk, *J. Phys. Chem. B* **2008**, *112*, 14415.
36. W. Song, C. R. K. Glasson, H. Luo, K. Hanson, M. K. Brennaman, J. J. Concepcion, T. J. Meyer, *J. Phys. Chem. Lett.* **2011**, *2*, 1808.
37. K. Hanson, M. K. Brennaman, A. Ito, H. Luo, W. Song, K. A. Parker, R. Ghosh, M. R. Norris, C. R. K. Glasson, J. J. Concepcion, R. Lopez, T. J. Meyer, *J. Phys. Chem. C* **2012**, *116*, 14837.

Graphical Abstract